The High Energy Transmission Grating Spectrometer for AXAF

T.H. Markert, C.R. Canizares, D. Dewey, M. McGuirk, C. Pak, M.L. Schattenburg

Center for Space Research
Massachusetts Institute of Technology
Cambridge, MA 02139

ABSTRACT

The High Energy Transmission Grating Spectrometer (HETGS) is one of the scientific instruments being developed for NASA's Advanced X-ray Astrophysics Facility (AXAF), scheduled for launch in 1998. The HETGS will be capable of measuring spectra with high resolution and sensitivity from a variety of compact and slightly extended cosmic X-ray sources.

In this paper we describe the overall design of the HETGS and its expected scientific performance. The HETGS consists of two arrays of gold grating elements (High-Energy gratings [HEGs] and Medium-Energy Gratings [MEGs] which are optimized for the energy ranges 0.8 - 10 keV [HEG] and 0.4 - 5keV [MEG]). The details of the grating elements and their fabrication methods are described in Schattenburg *et al.* (this conference). The gratings are mounted on a support plate which can be inserted immediately behind the AXAF telescope assembly. X-rays diffracted by the gratings are dispersed onto the focal plane detector strips which are components of either of the two AXAF imagers (the HRC or ACIS). The two kinds of gratings are oriented at a slight angle with respect to each other so that the dispersed spectra form a shallow "X" on the readout device. The gratings and detectors are mounted on a Rowland torus to correct for most of the optical aberrations. The grating-detector combination achieves resolving powers ($E/\Delta E$) as high as 1000 at some energies, and has significant effective area (10 - 200 square centimeters) for all energies 400 eV $<$ E $<$ 10 keV.

Keywords: X-ray astronomy, X-ray spectroscopy, transmission gratings, satellite astronomy

1 INTRODUCTION

The High Energy Transmission Grating Spectrometer (HETGS) is one of the two high-spectral spectral resolution instruments being developed for the Advanced X-ray Astrophysics Facility (AXAF), a NASA satellite scheduled for launch in 1998. The HETGS and a similar device optimized for lower energies (the Low Energy Transmission Grating Spectrometer or LETGS[1–3]) are spectrometer systems consisting of three components: the AXAF X-ray telescope (the High Resolution Mirror Assembly or HRMA, a set of 4 confocal, grazing-incidence, paraboloid-hyperboloid telescopes), the transmission grating arrays which are inserted immediately behind the mirror assembly, and the focal plane detector which reads out spectrum dispersed by the gratings. For AXAF, the two focal plane imaging devices are a CCD array (the ACIS or AXAF CCD Imaging Spectrometer[4,5] and a microchannel plate array (the HRC or High-Resolution Camera[6,7]).

The transmission gratings on AXAF are expected to provide high-resolution spectra of a wide range of point-like (or slightly spatially extended) astronomical objects. We anticipate that these sharp spectra will enable astrophysicists to employ the tools of plasma diagnostics (which usually require precise knowledge of flux from a number of individual X-ray emission line) to study the X-ray properties of stars, galactic nuclei, binary X-ray sources and, in some cases, supernova remnants and the hot gas trapped in clusters of galaxies. These (and other tools that have been developed over the past 30-some years) will enable scientists to determine, with reasonably high accuracy, the temperatures, ionization structures, ionization history, elemental abundances, and velocities (via the Doppler shifts) of the X-ray emitting plasmas. The techniques of high-resolution cosmic X-

ray spectroscopy have, in the past, been employed in studies of the sun and in a few dozen sources which have been bright enough to be accessible to earlier, less sensitive satellite instrumentation. With the spectrometers on AXAF we expect to extend these studies to hundreds of objects. For a general discussion of the prospects for high-resolution X-ray spectroscopy of cosmic plasmas, see Gorenstein and Zombeck.[8]

The HETGS investigation has been reviewed previously,[9,10] but has not been discussed in detail for several years.[11] In the last few years there have been a number of developments in the AXAF program, and several important changes in the HETGS design, that make a more comprehensive review appropriate at this time. This is the first in a series of four papers discussing the *current* status of the HETGS investigation. It will serve as a general introduction and overview of the experiment, concentrating on the overall design and operation of the instrument and showing some of the anticipated scientific capabilities. The next paper (Schattenburg *et al.*[12]) details the fabrication of the individual grating elements. Nelson *et al.*[13] describe studies of sample transmission grating elements made at a synchrotron, as well as the model for grating efficiency as a function of energy. Finally Dewey *et al.*[14] will discuss the methods of calibrating and verifying the performance of the entire complement of transmission grating elements (336 elements for the flight assembly as well as an equal number of spares) that we are planning to carry out at MIT.

2 INSTRUMENT DESCRIPTION

2.1 Overview

The High Energy Transmission Grating (HETG) is our nomenclature for the array of transmission grating elements that sits behind the HRMA and is one of the three components of the HETGS. Since the HETG is the part of the overall spectrometer that is built at and by MIT, we will concentrate on its design and properties in this paper.

The entire HETGS is shown schematically in Figure 1. X-rays are focussed by the HRMA. As they leave the telescope assembly they may be intercepted by a support structure onto which the grating elements are attached (the grating assembly is insertable and may be interchanged with the LETG assembly, or a contamination cover, see Figure 5; of course, if a direct image is desired, the pathway to the focus can remain unobstructed).

The X-rays pass through the individual grating elements and are diffracted according to the grating equation

$$m\lambda = p \times sin(\theta) \tag{1}$$

where m is the order of diffraction (an integer $0, \pm1, \pm2, ...$), p is the grating period and θ is the dispersion angle. The dispersed X-ray spectrum is then read out by one of the two imaging instruments.

The fundamental theory of transmission gratings is well known (see, for example, Born and Wolf[15]) The HETG instrument is unusual, however, in two respects (Schnopper *et al.*,[16] Canizares, Schattenburg and Smith[9]). First, since it operates in the X-ray regime, the grating period must be quite small so as to disperse the radiation a reasonable distance (the HETG gratings have periods of 4000 Åand 2000 Å). This presents a challenge in fabrication (see Schattenburg *et al.*[12] for a description of the nanofabrication techniques used to produce the gratings).

Second, because the X-radiation is penetrating, we can make use of the fact that the X-rays pass through the grating bars with only partial attenuation to customize the grating efficiencies. At some energies and for some thicknesses of the grating bars, the X-rays are phase-shifted by π and there is destructive interference in

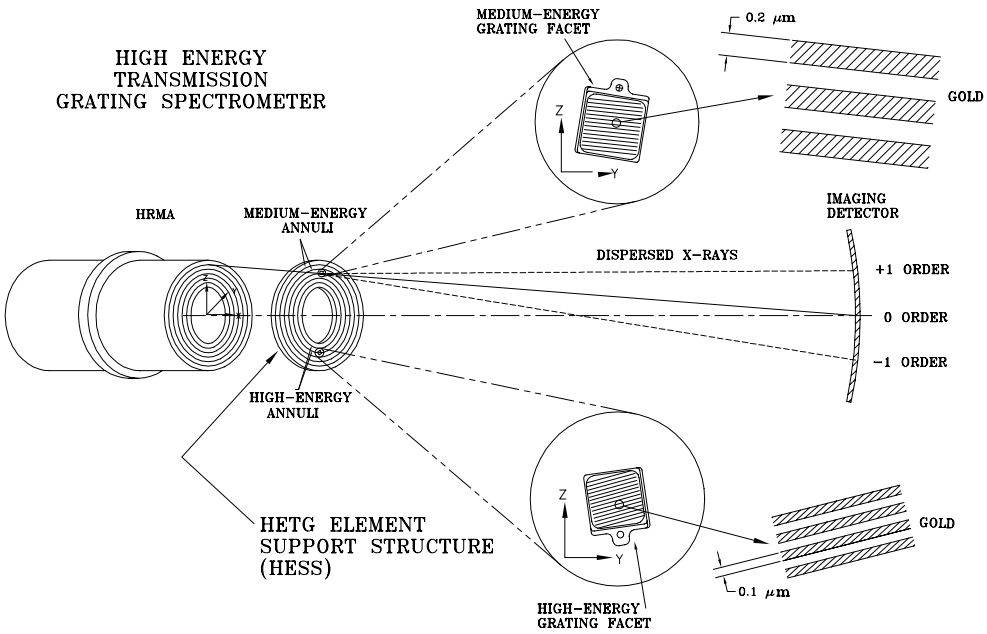

Figure 1: Schematic sketch of the AXAF High Energy Transmission Grating Spectrometer. The support structure is tiled with 192 MEG grating elements and 144 HEG elements. Each grating element is a square of approximately 6 cm^2 of active grating area mounted on an invar frame.

the direct beam ($m = 0$). The higher order ($m > 0$) radiation is thus enhanced. The efficiency model for the HETGS gratings is discussed in detail by Nelson *et al.*[13] The equations below[16] show the differences in efficiency for an infinitely thick (opaque) grating (equation 2) and for a grating of thickness t (equation 3), for the $m > 0$ cases. Clearly by selecting the thickness properly ($t = \frac{\lambda}{2\delta}$) one can enhance the efficiency at the wavelength of interest by up to a factor of four.

$$\eta_{opaque} = 2 \times \frac{sin^2(\frac{m\pi a}{p})}{m\pi^2} \tag{2}$$

$$\eta_{phased} = \eta_{opaque} \times [1 + e^{-2kt\beta} - 2e^{-kt\beta}cos(kt\delta)] \tag{3}$$

Here a is the width of the space between grating lines and p is the period. m is the order of diffraction, k is the wave number ($=2\pi/\lambda$) and (δ, β) are the energy-dependent optical constants (the real and imaginary parts of the index of refraction) of the grating material (gold for the HETG). Figure 2 illustrates the implications of these equations for real phased gratings. If the grating bars are 7000 Å thick (our goal for some of our gratings), then the first-order efficiency (sum of $m = 1$ and -1) increases significantly for energies above about 1.7 keV.

The individual grating elements are approximately 1 inch square, and are tiled on the HETG support plate (so-called HETG Element Support Structure or HESS) so as to intercept all of the X-rays reflecting off the HRMA (Figure 1). There are two kinds of grating elements, one set which is optimized for the higher AXAF energies (High Energy Gratings = HEGs, for roughly 0.8-10 keV) and a second set that is optimized for the middle part of the AXAF energy range (Medium Energy Gratings = HEGs for 0.4-5 keV). As indicated in Figure 1, the HEG gratings are assembled over the inner two mirror annuli and the MEGs over the outer two annuli. This configuration is chosen because most of the high-energy response of the the HRMA is in the inner two mirrors.

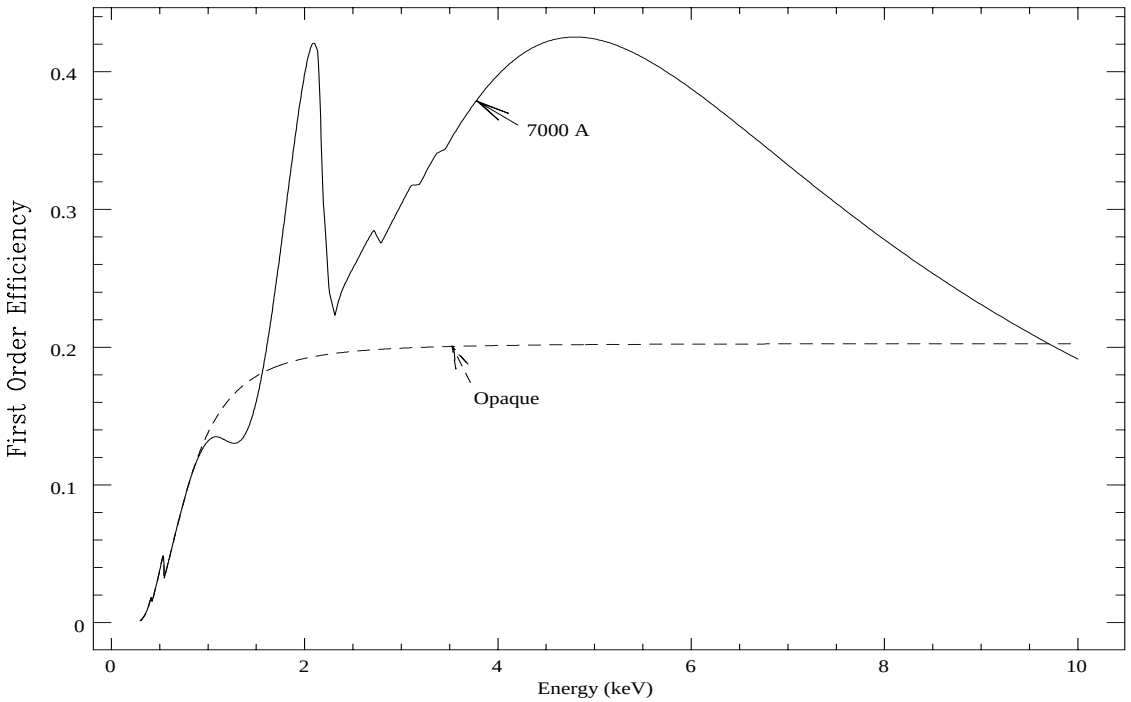

Figure 2: Comparison between theoretical efficiencies for an opaque and a phased transmission grating. The phased grating has the nominal parameters of the HETG High Energy Gratings (HEGs). Note the enhanced efficiency of the phased grating above about 1.7 keV. Both gratings are assumed to be mounted on polyimide support films. These films account for the drop-off in efficiency at low energies.

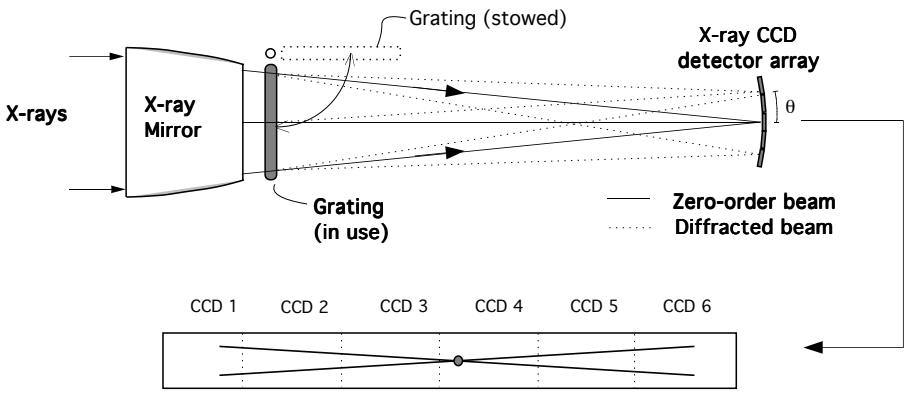

Figure 3: Another schematic version of the HETG. Here the grating insertion capability is shown explicitly. Also shown is the view along the optical axis showing the dispersion of the two grating types onto the imaging detector. base is not shown.

Both grating types disperse X-ray spectra into (slightly astigmatic) lines. However, since the gratings have different periods, the energy scales are different. Because it would be difficult to unravel overlapping spectra, we have arranged to tilt the HEGs and the MEGs with respect to one another so that the grating bars (and thus the dispersed spectra) are an angle of 10°. Figure 3 is another schematic diagram of the HETGS which shows the view of the dispersed X-rays on one of the imaging detectors (the CCD array, ACIS, is chosen). At the center of the array (slightly offset so that it doesn't fall between CCD chips) is the zeroth order (the undispersed X-rays). The other orders are then diffracted into the two lines as shown, making a shallow "X" on the CCD array. The HEG and MEG spectra can then be analyzed independently, or they can be summed (after applying the necessary corrections due to the differences in energy scale) if better statistics are desired.

2.2 Individual Grating Elements

The properties of the grating elements are summarized in Table 1. Both HEGs and MEGs are periodic structures of gold bars supported on polyimide membranes. Figure 3 shows a schematic of a single grating element. The polyimide film serves to support the grating bars, and is relatively transparent to X-rays above about 1 keV. The MEG gratings, which are intended for lower energies, will be supported by 0.5 microns of polyimide.

The grating/polyimide is glued to a metallic frame, as shown in Figure 4. The frame is made of invar, which has a low coefficient of thermal expansion. This choice of material prevents stress on the grating bars when the HETG is inserted into its operating position (at which point there can be a small but significant temperature change). The grating is further isolated from thermal stress by the way it is mounted: a small pad (not shown in the figure) extends from one side of the frame. A screw-hole in the pad is used for mounting onto the HESS. The pad cantilevers the frame off of the HESS surface, so that no thermal deformations of the support structure can transmit deformations to the individual frames.

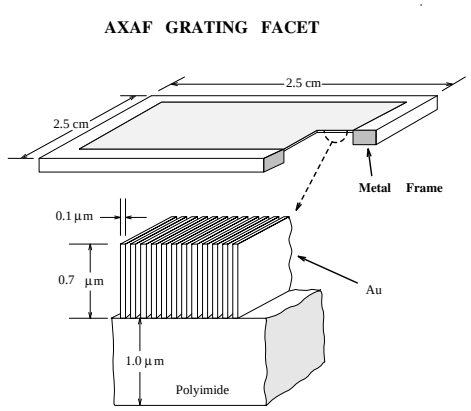

Figure 4: Schematic of an HEG grating in the HETGS. The gold bars are supported by the polyimide film (0.5 microns thick for the MEGs). A thin metallic plating base (few hundred microns) is present in the actual grating but is not shown in this sketch.

Figure 5 is a photograph of a sample MEG grating. The HEG gratings are slightly smaller (Table 1) but have a very similar appearance.

Table 1: Parameters of the High Energy Transmission Grating (HETG) Grating Elements

Parameter	High Energy (HEG)	Medium Energy (MEG)
Number Required	144	192
Size (side of square)	0.940 inch	1.035 inch
Dispersion Direction with respect to x axis	+5.0 degrees	-5.0 degrees
Period	0.2 microns	0.4 microns
Grating Bar Material	Gold	Gold
Grating Bar Height	0.7 microns	0.4 microns
Support Film	1 micron polyimide	0.5 micron polyimide

2.3 The HETG Element Support Structure (HESS)

The HETG Element Support Structure is plate onto which the individual transmission gratings are attached. The HESS, in turn, is attached to a yoke at three points which is connected to an insertion mechanism that allows the HESS to rotate into position immediately behind the HRMA. The HESS is machined from aluminum and, in the current design, weighs about 23 pounds (when fully populated with gratings).

Figure 5: Photograph of a sample MEG grating.

The HESS mechanical design is shown in Figure 6, with its full complement of 336 grating elements. It is 43.5 inches in diameter (exclusive of the yoke mounting pads). It is machined so that the grating elements lie on a "coma-corrected" surface. This surface is a Rowland torus[17] with a radius in the plane of dispersion of 4.325 meters (the Rowland circle radius), and a radius on the orthogonal plane of 8.65 meters (equal to the grating to focal-plane distance). Each facet is located on the torus, with its normal parallel to the local ray from the HRMA. The imaging detectors are also mounted on the Rowland circle at the focal plane (the detectors are composed of flat segments, 6 CCD chips for ACIS and three microchannel plate arrays for the HRC, so that the conformation to the Rowland circle, while adequate for minimizing the optical aberrations, is an approximation).

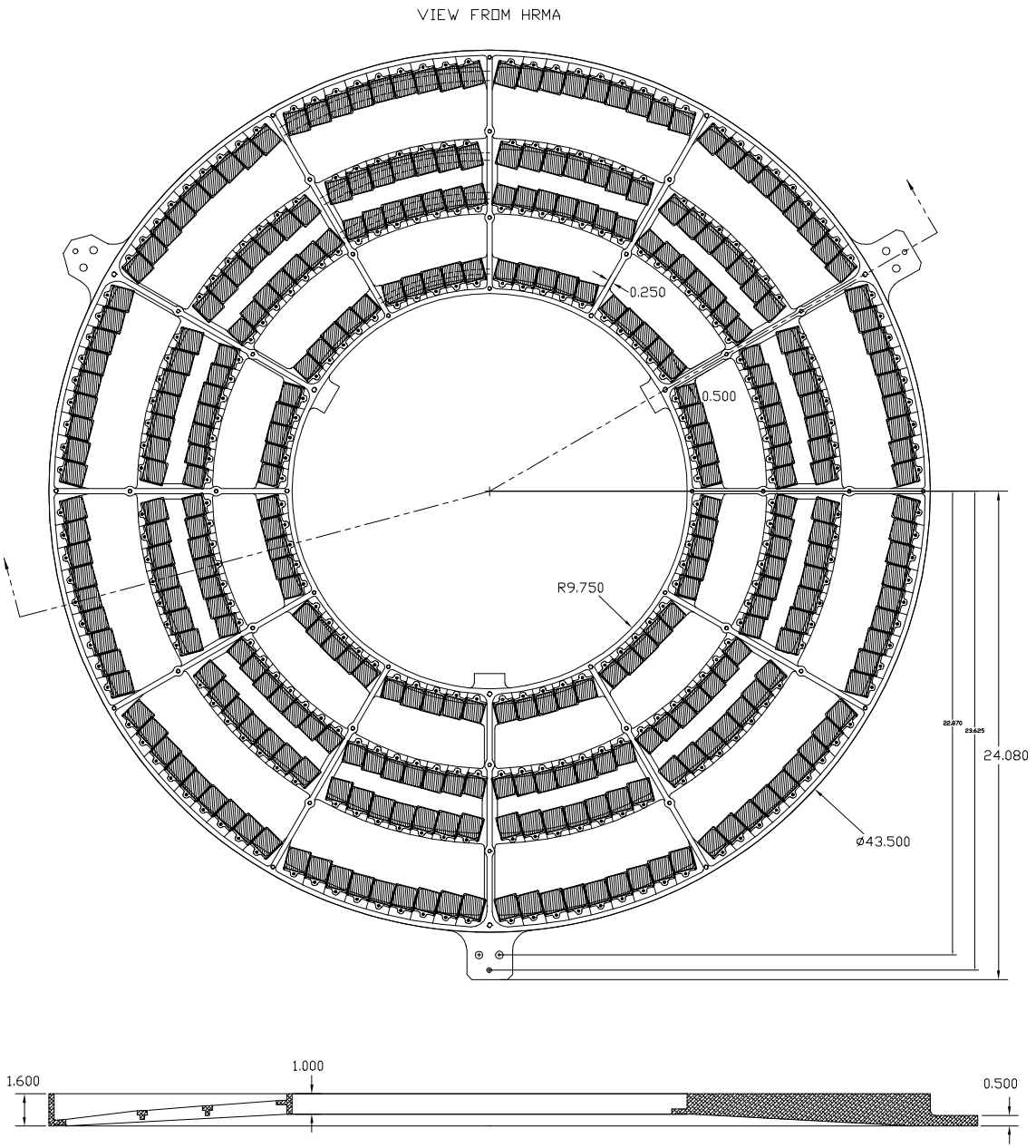

Figure 6: Engineering drawing of the HETG. The support structure (the HESS) is fully populated with 336 grating elements.

2.4 Fabrication of the HESS and alignment of the grating elements

The technique for fabricating the individual grating elements is described in detail in Schattenburg *et al.*[12] After the grating elements are made, tests are performed at MIT to measure the period, period variation, and efficiency of each of the individual gratings. These tests and the MIT facilities are described in Dewey *et al.*.[14]

When the MIT grating evaluation is complete, those gratings that meet the specifications on spectral resolving power and efficiency are assembled on the HESS. The grating elements must be co-aligned to within ~ 1 arc minute (i.e., the grating bars must be parallel from grating to grating within the specified tolerance). This alignment is achieved by taking advantage of the fact that gratings with periods this small act as almost perfect linear polarizers of optical light.[18] The polarization of a bright light is modulated periodically with a photoelastic modulator and then passed through an individual grating element to be detected by a photodiode. The detector is then read by a lock-in amplifier triggered by the modulation signal. The grating orientation is adjusted until a null is reached in the lock-in. All of the individual grating elements mounted on the HESS are adjusted with the same orientation.

Following assembly of the completed HESS, the HETG is delivered to the Marshall Space Flight Center for X-ray calibration with the HRMA and the flight detectors. When calibration is completed (now scheduled for 1997) the various components are shipped to the prime AXAF contractor, TRW, for the assembly of the spacecraft. Launch of AXAF is currently scheduled for 1998.

3 PROPERTIES OF THE HETGS

3.1 Spectral Resolving Power

The spectral resolving power of any spectrometer is given by

$$R \equiv E/\Delta E \tag{4}$$

where ΔE is the FWHM of the response of the spectrometer to a monochromatic X-ray line. One of the strengths of a grating spectrometer is the very high resolving powers that can be achieved. For R $\geq$ 1000 one can hope to resolve some of the very closely spaced X-ray emission lines that arise from hot astrophysical plasmas. Doppler shifts $\sim$ 300 km sec^{-1} can also be discerned with resolutions this high. Because of the scientific importance of achieving high resolving power, we have specified that the HETG (when used in an otherwise perfect system) would achieve R of 1000 or greater (at some energies in the range 0.4-10 keV).

For the HETGS it can be shown that

$$R \equiv E/\Delta E = y/\Delta y \tag{5}$$

where y is the dispersion distance and Δy is the blur of a monochromatic line (in the AXAF coordinate system the x-axis is the optical axis, y is the dispersion axis and z the cross-dispersion axis). The resolving power of the HETGS is a complex function of various parameters that can broaden a narrow line. At the higher end of the AXAF energy range, the line response function is dominated by the inherent blur of the HRMA mirrors, which limit the resolving power to a few hundred. As the energy decreases, however, other factors become important. Such things as the variation in the grating period within individual gratings, or slight errors in the shape of the

HESS can add significant blurring at the lower energies. It is at the lower energies, furthermore, where we can achieve the higher resolving powers. Consequently, we make a effort to control the various parameters over which we *have* control (i.e, the HETG geometry and fabrication quality) so as to achieve the desired resolutions.

We have constructed a comprehensive error budget for the HETGS resolving power, containing some 32 terms, over most of which we have some control. We have set limits on these terms consistent with our resolving power goals, and have demonstrated that these goals are achievable (for example, we can routinely limit variations in the period within a grating element, $\Delta p/p$, to less than 250 ppm).

Figure 7 shows the resolving power we expect to achieve with the HETGS, based on our error budgets. Also shown, for comparison, are the expected resolving powers for the other AXAF spectroscopic instruments.

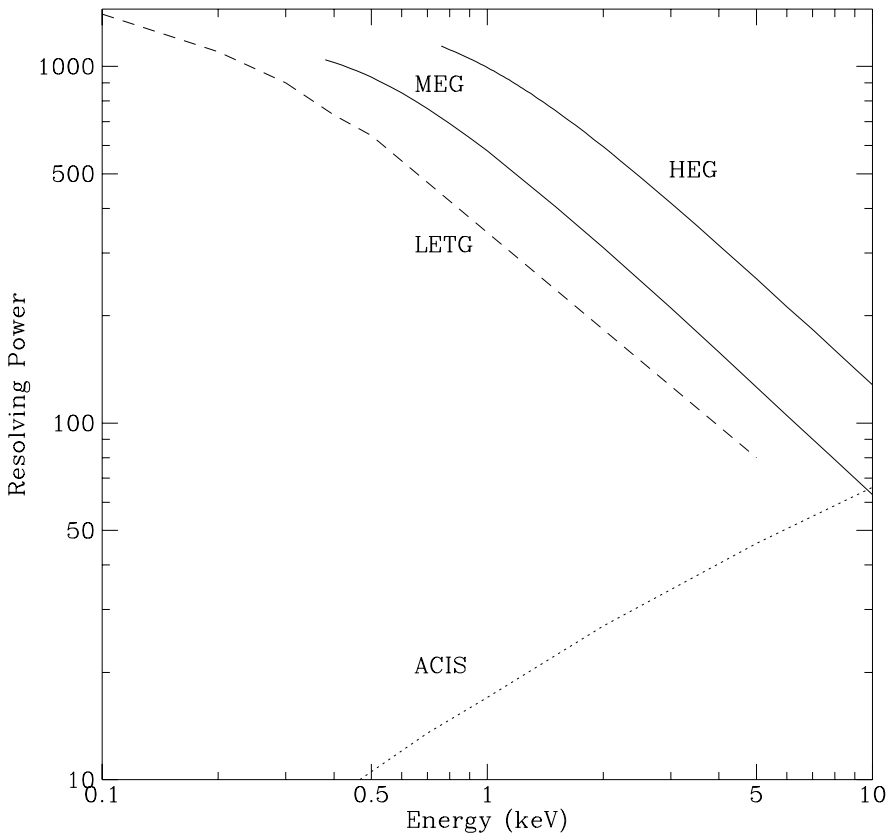

Figure 7: Resolving power of the various AXAF spectrometers as a function of energy

The resolving power curves and associated error budget apply to observations of *spatially unresolved* sources only (i.e., objects such as stars, galactic nuclei or binary X-ray source). For sources which are *extended*, however, the resolving power decreases rapidly, and essentially linearly with source extent. For example, a source 10 arc secs in diameter has a maximum resolving power $E/\Delta E$ of 150. Nevertheless, for some classes of objects, observations of this quality will be useful (for example, observations of supernova remnants in nearby galaxies). Studies of more extended objects, furthermore, which have bright knots or other relatively isolated features can also be productive. Even a resolving power of 20 or so (as might result from an observation of an object with an angular extent of some 1 arc min) will be superior to that achieved with ACIS at some energies.

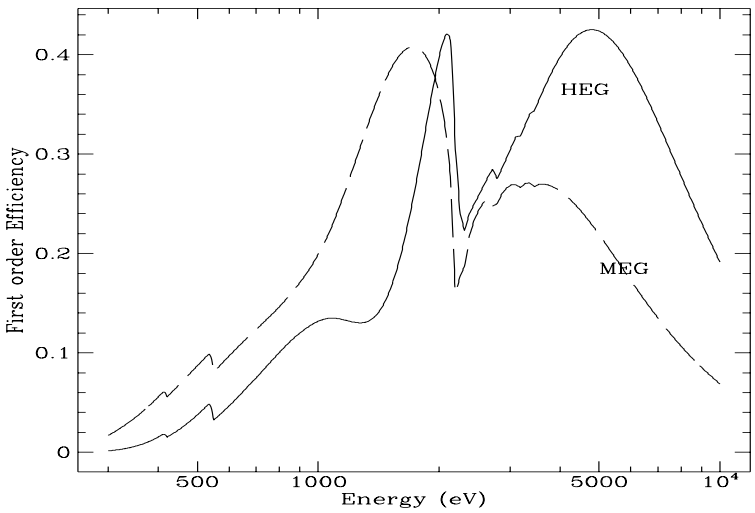

Figure 8: Efficiency of the HEG and MEG gratings with nominal grating parameters

3.2 Efficiency and Effective Area

As was noted above, the parameters of the HEGs and MEGs have been chosen to maximize the grating efficiency in particular regions of the AXAF energy range. Figure 8 illustrates the efficiencies of the two kinds of gratings (in the combined ±first orders) for the nominal grating parameters (Table 1). The curves were computed using a somewhat more sophisticated version of equation [3]. The model and the agreement of the model with data taken at a synchrotron are discussed by Nelson *et al.*[13]

The efficiencies of the HEGs and MEGs must be folded with the reflectivity of the HRMA and the quantum efficiencies of the detectors in order to determine the sensitivity of the HETGS as a whole. Figure 9 is a plot of the effective area of the overall HETGS.

The effective area curves are shown for the nominal ACIS and HRC detectors. Note that the ACIS detector combination is more sensitive at higher energies. The HRC has more lower energy response in part due to the natural response of the microchannel plate detectors and in part due to the longer physical dimensions of the HRC spectral readout (the dispersed spectrum falls off the end of the ACIS array before it falls off the HRC array). Depending on the goals of the particular investigation, the HETG observer will select either the HRC or ACIS as the appropriate readout device. Note also that these curves have assumed the nominal front-side illuminated CCD chips for ACIS. The ACIS team is working on a back-side illuminated alternative, which, if successful, will improve the ACIS response at lower energies.

3.3 Observations with the HETGS

As note above, the HETGS will be used primarily, but not exclusively, for studies of unresolved sources. In this section we present two simulations of HETG obseervations of star systems.

Figure 10 shows a simulated observation of the RS CVn system II Pegasi. This simulation uses the ACIS detector and adds together the HETG dispersed spectrum in both first orders and for both the HEG and MEG

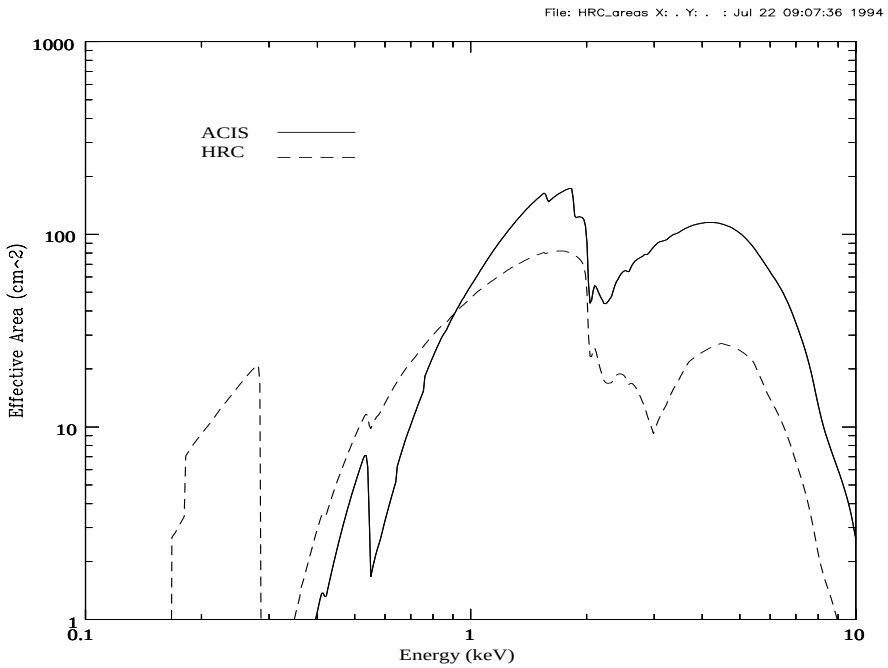

Figure 9: Effective areas of the HETGS for the nominal HRMA, HRC and ACIS response functions. The HETG response is employs the efficiencies in both first orders and sums together the spectra from both the HEG and MEG grating types

grating types. The observation time (14000 secs) was chosen to give about 10,000 total counts. This particular display is binned somewhat more crudely than would be the case for the actual HETGS, but it is illustrative of the number of counts and does show exhibit a large number of X-ray emission features.

Figure 11 shows another HETGS simulation, this time of the binary star system Capella. In this case, since Capella is a brighter source than II Peg, the simulation is for an observation of about 5 minutes. In addition, for this example we chose finer bin sizes (and a smaller energy range) in order to illustrate the advantage of high spectral resolution in separating closely spaced lines. This simulation employs, as usual, both the +first and the -first order data. Unlike the previous simulation, it uses the MEG gratings only. If the goal of the observation is to achieve the highest possible resolving power, then one would select either the HEG or MEG (as appropriate) and *not* sum them together (summing would degrade the resolution of the higher-resolution grating). If the goal is to achieve the largest number of counts in each line, then the HEG and MEG spectra would be summed (the resolution is not bad in this case however, as can be seen from Figure 7).

4 Acknowledgements

We are grateful for the contributions of the many engineers, technicians and students who have assisted in the design, development and testing of the HETG over the past 10 years. We note in particular the efforts of Gene Galton, the HETG Project Manager. The work presented here benefited greatly by the advice and suggestions of the HETG Science Issues group, notably Dave Huenemoerder, Herman Marshall, Joel Kastner, Mike Juda, and Peter Ford. This work was supported in part by NASA contract NAS8-38249.

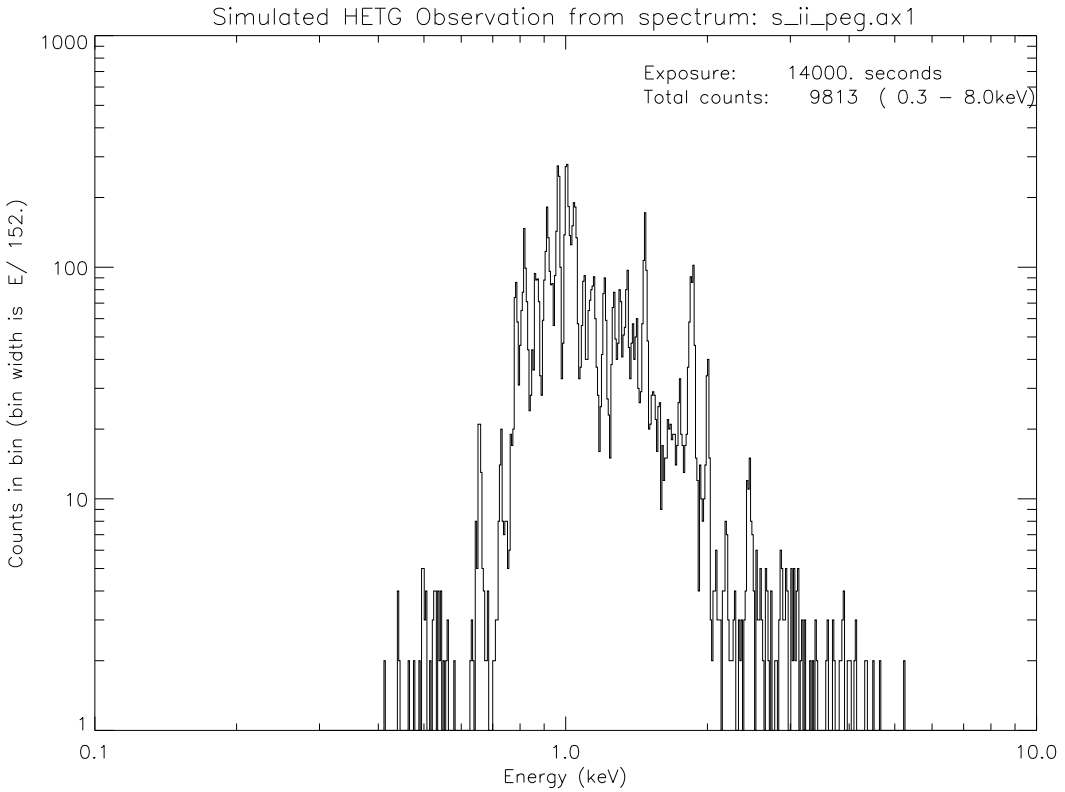

Figure 10: Simulated HETGS observation of the RS CVn system II Pegasi.

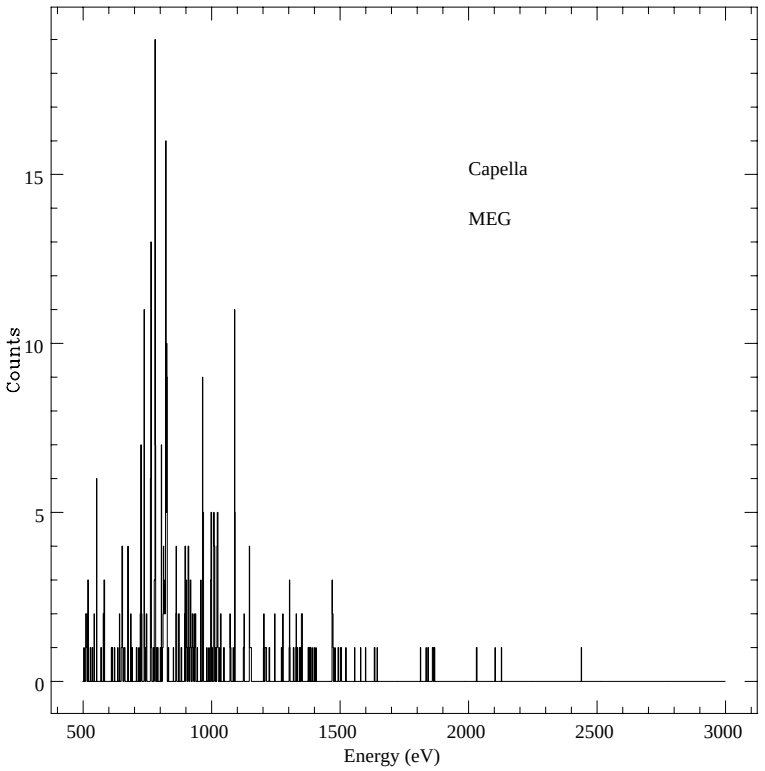

Figure 11: Simulated HETGS observation of the Capella. This simulation is for the MEG gratings only, and assumes a total observation time of 5 minutes.

5 REFERENCES

[1] A.C. Brinkman, J. J. van Rooijen, J.A.M. Bleeker, J.H. Dijkstra, J. Heise, P.A.J. de Korte, R. Mewe, and F. Paerels, "Low energy X-ray transmission grating spectrometer for AXAF", in *X-ray Instrumentation in Astronomy, Proc. SPIE*, vol. 597, pp. 232-240, 1985.

[2] A.C. Brinkman, *et al., Astro. Lett. and Communications*, Vol. 26, p. 73, 1987.

[3] T.H. Markert, "Dispersive Spectroscopy on AXAF", in *High-Resolution X-ray Spectroscopy of Cosmic Plasmas, IAU Colloquium No. 115*, P. Gorenstein and M. Zombeck, eds., pp. 339-344, Cambridge University Press, Cambridge, 1990.

[4] G.P. Garmire, *et al.*, "The AXAF CCD Imaging Spectrometer", in *X-ray Instrumentation in Astronomy, Proc. SPIE*, vol. 597, pp. 261-266, 1985.

[5] J.A. Nousek, G.P. Garmire, G.R. Ricker, S.A. Collins, and G.R. Reigler, *Astro. Lett. and Communications*, Vol. 26, p. 35, 1987.

[6] S.S. Murray and J.H. Chappell, "The Advanced X-ray Astrophysics Facility High Resolution Camera", in *X-ray Instrumentation in Astronomy, Proc. SPIE*, vol. 597, pp. 274-281, 1985.

[7] S.S. Murray, *et al.*, *Astro. Lett. and Communications*, Vol. 26, p. 113, 1987.

[8] P. Gorenstein and M. Zombeck, *High Resolution X-ray Spectroscopy of Cosmic Plasmas*, Cambridge University Press, Cambridge, 1990.

[9] Canizares, C.R., Schattenburg, M.L., and Smith, H.I., "The High Energy Transmission grating Spectrometer for AXAF", in *X-ray Instrumentation in Astronomy, Proc. SPIE*, vol. 597, pp. 253-260, 1985.

[10] C.R. Canizares, *et al.*, *Astro. Lett. and Communications*, Vol. 26, p. 87, 1987.

[11] M.L. Schattenburg, *et al.*, Optical Engineering, vol. 30, p. 1590, 1991.

[12] M.L. Schattenburg, R.J. Aucoin, R.C. Fleming, I. Plotnik, J. Porter, and H.I. Smith, "Fabrication of High Energy X-ray Transmission Gratings for AXAF", *these proceedings.*

[13] C.S. Nelson, T.H. Markert, Y.S. Song, M.L. Schattenburg, K.A. Flanagan, R.L. Blake, J. Bauer, E.M. Gullikson, "Efficiency Measurements and modelling of AXAF high energy Transmission Gratings", *these proceedings*

[14] D.Dewey, D.N. Humpheries, G.Y. McLean and D.A. Moschella, "Laboratory Calibration of X-ray Transmission Diffraction Gratings", *these proceedings.*

[15] M. Born and E. Wolf, *Principles of Optics, Sixth Ed.*, pp. 401-407., Pergamon, New York, 1980.

[16] H.W. Schnopper, *et al.*, "Diffraction Grating Transmission Efficiencies for XUV and Soft X-rays", *Appl. Optics*, Vol. 16, p. 1088, 1977.

[17] Beuermann, K.P., Brauninger, H., and Trumper, J., *App. Opt.*, vol. 17, no. 15., 2304, 1978.

[18] E.H. Anderson, A.M. Levine, and M.L. Schattenburg, "Transmission X-ray Diffraction Grating Alignment using a Photoelastic Modulator", *Applied Optics'*, vol. 27, pp. 3522-3525, 1988.